Effectiveness of Recent Fiber-interaction Diffusion Models for Orientation and the Part Stiffness Predictions in Injection Molded Short-fiber Reinforced Composites

Babatunde O. Agboola[a], David A. Jack[b], S. Montgomery-Smith[c]

[a]*Department of Mechanical Engineering, Baylor University, Waco, TX 76798, U.S.A.*
[b]*Department of Mechanical Engineering, Baylor University, Waco, TX 76798, U.S.A.*
[c]*Department of Mathematics, University of Missouri, Columbia MO 65211, U.S.A.*

Abstract

Two fiber interaction models for predicting the fiber orientation and resulting stiffness of a short-fiber reinforced thermoplastic composite are investigated, the isotropic rotary diffusion of Folgar and Tucker (1984) and the anisotropic rotary diffusion of Phelps and Tucker (2009). This study employs several fiber orientation tensor closure approximations for both diffusion models and results are compared to those from the numerically exact spherical harmonic approach. Results are presented for variations in the fiber orientation and the processed part stiffness. A significant difference was observed between the stiffness predicted by both rotary diffusion models. It is worth noting that not all closures behave the same between the diffusion models, thus encouraging further studies to refine and validate the new fiber interaction models and solution approaches. A study of the predicted flexural modulus is presented, and results suggest that flexural modulus experiments may aid in further refining the fiber interaction models.

Keywords: B. Directional Orientation B. Mechanical Properties C. Computational Modeling E. Injection molding

1. Introduction and overview of problem

Short-fiber reinforced thermoplastic composites have received widespread use due to the enhancement of the structural properties of a polymer component at a minimal cost. The fibers are suspended within the polymer matrix during processing and orient in response to the flow kinematics of the polymer melt. The motion and orientation of fibers is influenced

by the kinematics of the flow and by interactions with adjacent fibers. Thus the orientation of short-fibers in an injection molded composite will vary within the part, producing spatial inhomogeneity in the orientation and anisotropy of the mechanical properties. Accurate and efficient predictions of the orientation and the resulting material properties will be very useful for controlling and designing injection molding manufacturing processes to obtain suitable parts. Consequently, many researchers have developed models that accurately and efficiently predict the flow induced orientation of short fibers within a thermoplastic (see e.g., [1, 2, 3, 4, 5, 6]).

The Jeffery model [7] forms the basis for most models that predict the fiber orientation evolution within a composite and is valid for a single fiber in a thermoplastic melt of a dilute suspension. A thermoplastic is a non-Newtonian fluid, but over the length scale of the fiber the velocity gradients are effectively constant. Therefore a single shear is experienced by the entire fiber thus not violating the Jeffery assumption of a locally Newtonian fluid. Due to the overwhelming computational burden in quantifying the motion of every fiber within the melt, an orientation probability distribution function (ODF) is used to describe the orientation of collections of fibers (see e.g., [2, 8]). The ODF is a complete, unambiguous description of the fiber orientation state and can be calculated from the processing conditions. Typical approaches to solve the equation of motion of the ODF rely on the control volume approach (see e.g., Bay [3]) which take days to solve for simple flows (see e.g., [3, 9, 10, 11]). The control volume solution approach of Bay [3] has been considered to yield the most accurate solutions of the ODF. Recently, Montgomery-Smith *et al.* [12] introduced the computationally efficient spherical harmonic approach which yields identical results to those of the Bay approach, but reduces the computational time from days to minutes for the same flows. In principle the spherical harmonic approach can be incorporated within a finite element software package for cavity simulations of the flow, but the scope of the memory requirements along each streamline of the flow currently make it impractical for industrial use.

Advani and Tucker [2, 8], cast the evolution equation of the ODF in terms of the moments of the orientation distribution [2], and called the resulting form of these moments the orientation tensors. Solutions of the orientation tensor equation of motion for the flows along an individual streamline can be solved in a matter of seconds [11] and are concise enough to

be utilized in industrial finite element codes. The orientation tensor approach suffers from the need for a higher order tensor to solve the equation of change. This brings about the need for a closure approximation of a higher order tensor in terms of a lower order tensor [2]. Researchers have proposed various forms for closure approximations [8, 4, 13, 14, 15, 4, 16], where the effectiveness of each model has been demonstrated only on the particular fiber interaction model for which they were developed. Montgomery-Smith *et al.* [17, 18] recently proposed a new closure called the fast exact closure (FEC), which combines the efficiency of the commonly used hybrid closure [2] and the accuracy of the ORT closure [19]. In the present paper, all results will be compared to the spherical harmonic solutions obtained using the method in [12]. This approach was demonstrated to retain the full accuracy of the ODF solution and is only limited by the numerical precision of the computer. Thus the spherical harmonic solution is considered true, if one assumes the diffusion model itself from the governing equation is true. Thus one can objectively compare the spherical harmonic solutions between two fiber interaction models without any bias from the choice of closure.

For concentrated suspensions, a rotary diffusivity term D_r is added to Jeffery's form of the ODF to account for the interaction of fibers. Folgar and Tucker [1] suggested that D_r relates to a statistical parameter called the interaction coefficient C_I. This empirical parameter has values that increase with the concentration of the fiber-plastic suspension as well as the fiber aspect ratio. The Folgar-Tucker model is independent of direction and throughout the text will be called the isotropic rotary diffusion (IRD) model. The IRD model tends to over predict the orientation kinetics of the fibers (see e.g., [6]), but is widely available in commercial software packages used for the design of injection molds. To solve this problem of the alignment rate, researchers have tried to find ways to slow down the orientation kinetics using physically meaningful approaches. Wang *et al.* [20] recently proposed an objective diffusion model to slow the orientation kinetics, called the reduced strain closure (RSC) model. Phelps and Tucker [6] further improved on the RSC model by introducing a directional dependance to the fiber interactions through the diffusion term of the ODF equation of motion and compared their results to experimental observations.

It has been noted that the fiber orientation kinematics are coupled with the flow kinetics for densely packed flows (see e.g., [21, 22]), and several researchers have provided solutions

using the full coupled form of orientation and flow (see e.g., [19, 23, 24]). It has been demonstrated in Wang *et al.* [20] that the incorporation of the full fiber orientation/flow velocity coupling is insufficient in predicting the fiber orientation correctly, where the greater impact is the choice of diffusion model. In the present context, so as not to obfuscate the comparisons between fiber interaction models, we will neglect coupling to bring attention to the two classes of diffusion models themselves. Full simulations of industrial injection molded composites will need to include the full coupling as well as selecting the proper fiber interaction model. The interested reader is encouraged to read Verweyst and Tucker [19] and Chung and Kwon [23] for extensive studies of the impact the full coupling has on the processed part stiffness when one uses the IRD fiber interaction model.

Advani and Tucker [8] linked the stiffness of the solidified part to the underlying orientation microstructure using an orientation averaging approach. Jack and Smith [25] derived the stiffness expectation from the fourth-order orientation tensor along with the variance of the stiffness, which is a function of the eighth-order orientation tensor. The relationship between the orientation tensor and the resulting stiffness was validated by Caselman [26] and was used by Gusev *et al.* [27, 28]. Recently, Nguyen *et al.* [29] used the anisotropic rotary diffusion (ARD) model by Phelps and Tucker [6] with the ORT closure to predict the stress/strain response for injection molded long fiber thermoplastics. Although their results are quite impressive, it is unclear to what extent the closure choice may bias the solution.

The objectives of this paper are, (1) to compare the IRD and the ARD diffusion models using the numerically exact spherical harmonic approach, (2) investigate the impact the choice of diffusion model has on the resulting stiffness, the natural frequency, and the flexural modulus of the processed composite, and (3) to investigate if the preferred closure for solving the orientation kinetics may be different between the two diffusion models.

2. Fiber Orientation Modeling

The study of the motion of short fibers in a fluid is often based on the motion of an individual particle using Jeffery's model [7] which captures the motion of rigid ellipsoidal particles through the equation of change for the unit direction vector $\mathbf{p}$ along the major axis. For typical industrial use, the modeling of individual fibers is computationally imprac-

tical, instead the fiber orientation distribution function $\psi(\mathbf{p})$, which will be call the ODF throughout the text, is used to describe the fiber orientation. The motion of a fiber within a concentrated suspension will be impeded by the motion of the neighboring fibers. This has lead to the development of interaction parameters often lumped into a rotary diffusion term D_r of the constitutive equation popularized by Bird *et al.* [30] (sometimes referred to as the generalized Fokker-Planck or the Smoluchowski equation) as

$$\frac{D\psi}{Dt} = -\frac{1}{2}\nabla_{\mathbf{p}} \cdot \left(\mathbf{\Omega} \cdot \mathbf{p} + \lambda \left(\mathbf{\Gamma} \cdot \mathbf{p} - \lambda \mathbf{\Gamma} : \mathbf{ppp}\right)\psi\right) + \nabla_{\mathbf{p}} \cdot \nabla_{\mathbf{p}}(D_r \psi) \tag{1}$$

where the fiber is assumed to move with the the bulk motion of the fluid, and ψ is regarded as a convected quantity. In Equation (1), $\nabla_{\mathbf{p}}$ is the gradient operator on the surface of a unit sphere (i.e., the gradient operator in orientation space), $\dot{\mathbf{p}}$ is the material derivative of $\mathbf{p}$ defined as $\frac{D\mathbf{p}}{Dt} = \frac{\partial \mathbf{p}}{\partial t} + \mathbf{v} \cdot \nabla$. The tensor $\mathbf{\Gamma} = \nabla \mathbf{v} + \nabla \mathbf{v}^{\mathrm{T}}$ is the rate of deformation of the surrounding fluid, $\mathbf{\Omega} = \nabla \mathbf{v} - \nabla \mathbf{v}^{\mathrm{T}}$ is the vorticity tensor of the fluid, $\mathbf{v}$ is the fluid velocity, and λ is a function of the equivalent ellipsoidal fiber aspect ratio a_e (see e.g., [31] on computing a_e for cylindrical and various other shaped fibers). The isotropic and an anisotropic form of the rotary diffusion term D_r will be discussed later in this text.

The spherical harmonic expansion of $\psi(\theta, \phi)$ proposed by Montgomery-Smith *et al.* [12] yields a numerically exact systematic approach for solving the ODF of Equation (1). This approach expands the orientation distribution function, $\psi(\mathbf{p})$, using the complex spherical harmonics Y_l^m to any desired order as

$$\psi(\mathbf{p}) = \sum_{l=0}^{\infty} \sum_{m=-l}^{l} \hat{\psi}_l^m(\mathbf{p})\, Y_l^m \tag{2}$$

where Y_l^m are the complex spherical harmonic coefficients and $\hat{\psi}_l^m$ contain information pertaining to the orientation. The equation of motion for $\psi(\mathbf{p})$ is expanded using Equation (2) and numerically exact transient solutions, limited only by machine precision, of $\frac{D\psi}{Dt}$ may be obtained using the spherical harmonic expansion. This new algorithm is exceptionally efficient as compared to solutions using the control volume method presented by Bay [3], where the control volume approach requires 2-3 orders of magnitude more time than the numerically exact spherical harmonic approach.

The form of the spherical harmonic solution could be implemented into commercial finite element solutions of the ODF that may vary in both space and time, but the number of degrees of freedom at each node make it impractical. Most industrial simulations use the orientation tensor approach popularized by Advani and Tucker [2], where the second- and the fourth-order orientation tensor components are defined as

$$\begin{aligned} \mathbf{A} &= \oint_S \mathbf{pp}\, \psi(\mathbf{p})\, d\mathbf{p} \\ \mathbb{A} &= \oint_S \mathbf{pppp}\, \psi(\mathbf{p})\, d\mathbf{p} \end{aligned} \tag{3}$$

where $\oint_S (...)\, d\mathbf{p}$ represents the integral on the unit sphere encompassing all possible fiber orientations, $p_i p_j$ is the tensor (or dyadic) product of the fiber orientation vector $\mathbf{p}$ with itself. Orientation tensors are completely symmetric, i.e. $A_{ij} = A_{ji}$ and $\mathbb{A}_{ijkl} = \mathbb{A}_{jikl} = \mathbb{A}_{klij} = \ldots$.

2.1. Isotropic rotary diffusion (IRD)

The Folgar-Tucker isotropic rotary diffusion (IRD) fiber interaction model is based on the assumption that all fibers in a melt interact with adjacent fibers in the same way, regardless of the direction a fiber is pointing. They define D_r from Equation (1) as $C_I G$, where C_I is called the interaction coefficient empirically determined by comparing experimental data and numerical predictions, and G is the scalar magnitude of the rate of deformation tensor defined as $G = \sqrt{\frac{1}{2}\mathbf{\Gamma} : \mathbf{\Gamma}}$. The results obtained using the IRD model predict steady fiber alignment states consistent with experimental observations [6] where the equation of motion for $\mathbf{A}$ may be expressed as (see e.g., [2])

$$\frac{D\mathbf{A}}{Dt} = -\frac{1}{2}(\mathbf{\Omega}\cdot\mathbf{A} - \mathbf{A}\cdot\mathbf{\Omega}) + \frac{1}{2}\lambda(\mathbf{\Gamma}\cdot\mathbf{A} + \mathbf{A}\cdot\mathbf{\Gamma} - 2\mathbf{\Gamma} : \mathbb{A}) + 2C_I G(\mathbf{I} - 3\mathbf{A}) \tag{4}$$

Observe in Equation (4), $\mathbb{A}$ appears in the equation of motion for $\mathbf{A}$. Similarly, the motion equation motion for $\mathbb{A}$ has the sixth-order orientation tensor (see e.g., [9]). The orientation tensor equation of motion for an even ordered tensor will contain the next higher even-ordered orientation tensor (see e.g., [32]). Therefore, to solve Equation (4) a closure will be required where $\mathbb{A}$ is approximated as a function of $\mathbf{A}$.

2.2. Anisotropic rotary diffusion (ARD-RSC)

Development of anisotropic rotary diffusion (ARD) models has been motivated by attempts to improve on the IRD model, which over predicts the fiber alignment rate observed

experimentally. Unlike the IRD, the ARD models take into account the directional dependence of fiber-fiber interactions, and there exist several ARD models in the literature (see e.g., Koch [5], Jack [32], Fan *et al.* [33], Phan-Thien *et al.* [34], and Wang *et al.* [20]).

The most recent ARD model of Phelps and Tucker [6] sought to improve upon the Reduced Strain Closure (RSC) diffusion model of Wang *et al.* [20], and the Phelps and Tucker ARD-RSC model was shown to be in reasonable agreement with experimental observations. The Phelps and Tucker ARD-RSC equation of motion for $\mathbf{A}$ can be expressed as [6]

$$\begin{aligned}\frac{D\mathbf{A}}{Dt} &= \frac{1}{2}\left(\boldsymbol{\Omega}\cdot\mathbf{A}-\mathbf{A}\cdot\boldsymbol{\Omega}\right)+\frac{1}{2}\lambda\left\{\boldsymbol{\Gamma}\cdot\mathbf{A}+\mathbf{A}\cdot\boldsymbol{\Gamma}-2\left[\mathbb{A}+(1-\kappa)\left(\mathbb{L}-\mathbb{M}:\mathbb{A}\right)\right]:\boldsymbol{\Gamma}\right\}\\ &+\dot{\gamma}\{2[\mathbf{C}-(1-\kappa)\mathbb{M}:\mathbf{C}]-2\kappa(\mathrm{tr}\mathbf{C})\mathbf{A}-5(\mathbf{C}\cdot\mathbf{A}+\mathbf{A}\cdot\mathbf{C})+10[\mathbb{A}+(1-\kappa)\left(\mathbb{L}-\mathbb{M}:\mathbb{A}\right)]:\mathbf{C}\}\end{aligned} \quad (5)$$

where the second order tensor $\mathbf{C}$ is defined in terms of the empirical coefficients b_i as

$$\mathbf{C} = b_1\dot{\gamma}\mathbf{I}+b_2\dot{\gamma}\mathbf{A}+b_3\dot{\gamma}\mathbf{A}^2+\frac{b_4}{2}\boldsymbol{\Gamma}+\frac{b_5}{4\dot{\gamma}}\boldsymbol{\Gamma}^2 \quad (6)$$

Note that the values of $\frac{1}{2}$ and $\frac{1}{4}$ that occur in Equation (6) differ from those given in Phelps and Tucker [6] in that they use $\frac{1}{2}\boldsymbol{\Gamma}$ to define the rate of deformation tensor. An alternative form is presented in [12], both for the equation of motion for $\mathbf{A}$ and for the equation of motion of $\psi(\mathbf{p})$ that can be numerically solved using spherical harmonics. For simple shear flow the coefficients b_i in Equation (6) were fit in [6] to the experimental observations from a plaque flow as

$$\mathbf{b} = \left[1.924\times10^{-4}, 5.839\times10^{-3}, 4.0\times10^{-2}, 1,168\times10^{-5}, 0\right] \quad (7)$$

It is important to emphasize that these parameters will work for the identical flow conditions in which they were fit (i.e., fiber packing density, flow viscosity, fiber aspect ratio, etc.), but for general implementations an exhaustive study must be performed to quantify the link between the coefficients b_i and any industrial implementation.

In Equation (5) the parameter κ will vary based on the degree of reduction of the orientation alignment rate desired, and we use the value of $\kappa = 1/30$ suggested by Phelps and Tucker [6]. The two fourth-order tensors $\mathbb{M}$ and $\mathbb{L}$ in Equation (5) are functions of the eigenvalues $A_{(i)}$ and eigenvectors $\mathbf{n}_i$ of $\mathbf{A}$ as

$$\mathbb{M} = \sum_{i=1}^{3}\mathbf{n}_i\mathbf{n}_i\mathbf{n}_i\mathbf{n}_i, \quad \text{and} \quad \mathbb{L} = \sum_{i=1}^{3}A_{(i)}\mathbf{n}_i\mathbf{n}_i\mathbf{n}_i\mathbf{n}_i \quad (8)$$

2.3. Closure Approximations

The equation of motion for the second-order orientation tensor for both diffusion models, e.g., Equations (4) and (5), contains the next higher even order orientation tensor. This brings about the need for a closure approximation to obtain a closed set of equations which may be generalized in component form as

$$\mathbb{A}_{ijkl} \approx \mathbb{F}_{ijkl}(\mathbf{A}) \tag{9}$$

where $\mathbb{F}_{ijkl}$ is a fourth-order tensor function operating on the second-order orientation tensor $\mathbf{A}$. An objective closure will be independent of the choice of coordinate frame [4]. Based on the symmetric nature of the orientation tensors defined in Equation (3), a fourth-order orientation tensor will have at most 15 independent components (which is further reduced to 14 due to the fact that $\mathbb{A}_{iijj} = A_{ii} = 1$, sum on i and j).

2.3.1. Hybrid Closure

The hybrid closure [2] is a popular closure in part due to its algebraic simplicity and computational efficiencies, despite some well known drawbacks in over predicting the alignment state [35]. It is formed from a linear combination of the quadratic closure of Doi [13] and the linear closure of Hand [14] as

$$\mathbb{A}_{ijkl} = (1 - f)\hat{\mathbb{A}}_{ijkl} + f\bar{\mathbb{A}}_{ijkl} \tag{10}$$

where $\hat{\mathbb{A}}_{ijkl}$ is the linear closure and $\bar{\mathbb{A}}_{ijkl}$ is the quadratic closure.

2.3.2. Orthotropic Closure (ORT)

The orthotropic closure approximations have significantly improved on the accuracy of the hybrid closure, but often at the cost of an increase in computational efforts (see e.g., [4, 36, 37, 38]). The orthotropic closures, first proposed by Cintra and Tucker [4], construct fitted forms of Equation (9) that rely on the invariants or the eigenvalues of the second-order orientation tensor. The construction of the orthotropic closures constrain the principal axis of the fourth-order orientation tensor to align with those of the second-order orientation tensor. The orthotropic closures typically provide the most accurate results when compared

to experimentally measured fourth-order orientation tensors [39]. The ORT closure used by VerWeyst and Tucker [19] is given as

$$\bar{\mathbb{A}}_{mm}^{closure} = C_m^1 + C_m^2 A_{(1)} + C_m^3 [A_{(1)}]^2 + C_m^4 A_{(2)} + C_m^5 [A_{(1)}]^2 + C_m^6 A_{(1)} A_{(2)} \tag{11}$$

where C_m^i are found by fitting the orientation tensor components from results obtained by full numerical solution of $\frac{D\psi}{Dt}$, and $A_{(1)} \geq A_{(2)} \geq A_{(3)} \geq 0$ with $A_{(1)} + A_{(2)} + A_{(3)} = 1$.

2.3.3. Neural Network Based Closure

The original Neural Network Based Closure (NNET) by Jack *et al.* [16] is based on the artificial neutral network (ANN) fitting technique which mimics the biological signal processing scheme. The Neural Network Orthotropic Closure (NNORT) closure [10] improves on the NNET in that it is truly objective and coordinate frame invariant. It combines the architecture of the ANN and maintains the principles of the orthotropic closures. Both the NNET and the NNORT are based on a network where the output is computed as

$$\bar{\mathbf{A}}_4 = f_2(\mathbf{w}_2 \cdot f_1(\mathbf{w}_1 \cdot \bar{\mathbf{A}}_2 + \mathbf{b}_1) + \mathbf{b}_2) \tag{12}$$

where $\bar{\mathbf{A}}_4$ and $\bar{\mathbf{A}}_2$ are, respectively, the independent values of $\mathbb{A}$ and $\mathbf{A}$, $\mathbf{w}_1$ and $\mathbf{w}_2$ are the network weights, $\mathbf{b}_1$ and $\mathbf{b}_2$ are the network biases, and f_1 and f_2 are, respectively, the hyperbolic tangent transfer function and the pure linear transfer function. The dimensions of each of the parameters in Equation (12) differ between the NNET and the NNORT, where the weights and the biases are obtained through a training algorithm of architecture based on known inputs and outputs obtained by full solutions of Equation (1) for the IRD fiber interaction model.

2.3.4. Fast Exact Closure (FEC)

The Fast Exact Closure (FEC) [18, 17] is not a closure approximation in the traditional sense as it does not rely on an approximation for $\mathbb{A}$, but it will yield exact solutions of the fiber orientation state in the absence of diffusion. The FEC has computational speeds comparable to that of the hybrid closure for a variety of diffusion models. The FEC does not rely on any curve fitting techniques, nor does it rely directly on an elliptic integral computation. The approach bypasses the fitting process of the orthotropic and the neural

network closures, and thus may be constructed independent of the diffusion model selected for the fiber interaction form used in many of the fitting methods. The FEC is generated by simultaneously solving the ODE's for two symmetric second-order tensors $\mathbf{A}$ and $\mathbf{B}$, where $\mathbf{A}$ is the second-order orientation tensor as defined in Equation (3). The FEC solution for the IRD fiber interaction model is expressed as

$$\begin{aligned} \frac{D\mathbf{A}}{Dt} &= \frac{1}{2}\mathbb{C} : [\mathbf{B} \cdot (\boldsymbol{\Omega} + \lambda\boldsymbol{\Gamma}) + (-\boldsymbol{\Omega} + \lambda\boldsymbol{\Gamma}) \cdot \mathbf{B}] + D_r(2\mathbf{I} - 6\mathbf{A}) \\ \frac{D\mathbf{B}}{Dt} &= -\frac{1}{2}(\mathbf{B} \cdot (\boldsymbol{\Omega} + \lambda\boldsymbol{\Gamma}) + (-\boldsymbol{\Omega} + \lambda\boldsymbol{\Gamma}) \cdot \mathbf{B}) - D_r\mathbb{D} : (2\mathbf{I} - 6\mathbf{A}) \end{aligned} \tag{13}$$

Notice in Equation (13) that there is no need for the classical closure as depicted in Equation (9) as there is no $\mathbb{A}$ appearing in either of the equations of motion. Alternatively there are two fourth-order conversion tensors $\mathbb{C}$ and $\mathbb{D}$. The two tensors convert between $\frac{D\mathbf{A}}{Dt}$ and $\frac{D\mathbf{B}}{Dt}$ using $\frac{D\mathbf{A}}{Dt} = -\mathbb{C} : \frac{D\mathbf{B}}{Dt}$ and $\frac{D\mathbf{B}}{Dt} = -\mathbb{D} : \frac{D\mathbf{A}}{Dt}$ (see e.g., [18]). The tensor $\mathbb{C}$ can be obtained directly from the eigenvalues of $\mathbf{A}$ and $\mathbf{B}$ (see e.g [18, 17]) and $\mathbb{D}$ is the rank-four tensor that is the tensor inverse of $\mathbb{C}$. The form of the equations of motion for the ARD-RSC, along with several alternative anisotropic diffusion forms, is given in Montgomery-Smith *et al.* [18, 17].

2.4. Material Properties Predictions

Injection molded composites consist of misaligned fibers and using homogenization, the composite stiffness can be expressed as a function of the fiber orientation and the underlying unidirectional stiffness tensor [2, 25]. For unidirectional composites with discontinuous reinforcements, Gusev *et al.* [40, 28] and Tucker and Liang [41] demonstrated that the Tandon-Weng model [42] yields reasonable predictions of the stiffness and will be used within the present paper. From this unidirectional stiffness tensor we use the orientation averaging approach suggested by Advani and Tucker [2] to predict the stiffness variation due to randomness in the fiber orientation within the composite. The orientation averaging form of an injection molded short fiber reinforced composite stiffness tensor is given as [2, 25]

$$\begin{aligned} \langle C_{ijkl} \rangle = \beta_1(\mathbb{A}_{ijkl}) + \beta_2(A_{ij}\delta_{kl} + A_{kl}\delta_{ij}) + \beta_3(A_{ik}\delta_{jl} + A_{il}\delta_{jk} + \\ A_{jl}\delta_{ik} + A_{jk}\delta_{il}) + \beta_4(\delta_{ij}\delta_{kl}) + \beta_5(\delta_{ik}\delta_{jl} + \delta_{il}\delta_{jk}) \end{aligned} \tag{14}$$

where the $\beta_i's$ are scalars related to the underlying unidirectional stiffness tensor as

$$\begin{aligned}
\beta_1 &= C_{1111} + C_{2222} - 2C_{1122} - 4C_{1212} \\
\beta_2 &= C_{1122} + C_{2222} \\
\beta_3 &= C_{1212} + \frac{1}{2}(C_{2233} - C_{2222}) \\
\beta_4 &= C_{2233} \\
\beta_5 &= \frac{1}{2}(C_{2222} - C_{2233})
\end{aligned} \tag{15}$$

Once the stiffness is known, the material stiffness constants are readily extracted (see e.g., Jones [43]), such as E_{ii} ($i = 1, 2, 3$ and no sum on i), G_{ij} ($i, j = 1, 2, 3$ and $i \neq j$), and ν_{ij} ($i, j = 1, 2, 3$ and $i \neq j$), which are, respectively, the Young's modulus along the x_i axis, the Shear modulus in the $x_i - x_j$ plane and the Poisson's Ratio on the x_i face in the x_j direction.

Notice in Equation (14) the appearance of $\mathbb{A}_{ijkl}$ as well as A_{ij}. When solving the equation of motion for the second-order orientation tensor, which already requires the use of a closure to approximate $\mathbb{A}_{ijkl}$, it is customary to use the same closure in the material stiffness calculation to compute C_{ijkl} of the fully hardened composites, but this is by no means a requirement. For the orientation evolution of A_{ij} from the FEC closure, in Equation (13), notice only $\mathbf{A}$ and $\mathbf{B}$ appear, both second order tensors and nowhere is $\mathbb{A}$ directly computed. As discussed in Montgomery-Smith *et al.* [17], the second-order orientation tensor $\mathbf{A}$ and the fourth-order orientation tensors are integral functions of the tensor $\mathbf{B}$ as

$$\mathbf{A} = \frac{1}{2}\int_S \frac{\mathbf{pp}}{4\pi\left(\mathbf{B} : \mathbf{pp}\right)^{3/2}} d\mathbf{p}, \qquad \text{and} \qquad \mathbb{A} = \frac{1}{2}\int_S \frac{\mathbf{pppp}}{4\pi\left(\mathbf{B} : \mathbf{pp}\right)^{3/2}} d\mathbf{p} \tag{16}$$

In Equations (2.12) - (2.14) of [17], analytic methods were presented to provide closed form solutions of the integral for $\mathbb{A}$ in terms of the eigenvalues of $\mathbf{B}$ and $\mathbf{A}$, and these expressions are used in the present study to compute $\mathbb{A}$ for use in the material stiffness calculation.

3. Results

We studied both the IRD and the ARD-RSC fiber interaction models using five different closure approximation methods: the commonly used Hybrid Closure (Hybrid) [2], the Orthotropic Closure (ORT) [19], the Neural Network Closure (NNET) [16], the Neural Network

Orthotropic Closure (NNORT) [10], and the Fast Exact Closure (FEC). For each flow studied, the closure results are compared to the numerically exact solutions from the spherical harmonic approach. Both orientation and the material stiffness results are compared for each flow. Typically, the predicted orientation among solutions approaches is compared as it contains the information required to construct the material stiffness. As will be demonstrated in the following results it is not always clear which closure will perform best, and whether best is defined as representing the orientation or representing the final processed part's stiffness. For each flow, the fiber is assumed to have an equivalent aspect ratio of $a_e = 10$, thus the geometry parameter in Equation (1) is $\lambda = \frac{(10^2-1)}{(10^2+1)} \approx 0.98$. The stiffness of the solidified part is computed using the Tandon-Weng model for the unidirectional elastic properties and the orientation averaging is performed using Equation (14) for a fiber and matrix Young's modulus of, respectively, $E_f = 30$GPa and $E_m = 1$GPa, a fiber and matrix Poisson's ratio of, respectively, $\nu_f = 0.2$ and $\nu_m = 0.38$ and a volume fraction of fibers $V_f = 0.2$ as discussed in [41]. For ease of comparison, the fiber orientation is randomly oriented at time $Gt = 0$.

3.1. Simple Shear Flow

The first set of results studied are for a simple shearing flow with fluid velocity vector components given as $v_1 = Gx_3, v_2 = v_3 = 0$, where G is the scalar magnitude of the rate of deformation tensor. Simple shear flow is chosen due to its regular occurrence in injection molded parts. The first set of orientation results presented is from the IRD fiber interaction model for an interaction coefficient of $C_I = 10^{-2}$, a commonly used value of C_I, and they are given in Figure 1(a). The solution using the spherical harmonic approach is numerically exact and the perfect closure would yield an orientation state that exactly mimics the spherical harmonic solution. As can be noted in Figure 1(a) the ORT, NNET, NNORT and FEC are nearly indistinguishable from each other, whereas the hybrid closure significantly over predicts the alignment state along the x_1 axis as indicated by the large A_{11} values. This trend is also observed when the orientation is used to predict E_{11} from the stiffness tensor using Equation (14), as shown in Figure 1(b). The results in Figure 1(b) are representative of a solidified composite if the flow were turned off at time Gt. To quantify the error in predicting the material stiffness component we define the time averaged relative error as the

ratio between the spherical harmonic results and the closure results as

$$\chi_{E_{11}}^{\text{Closure}} = \frac{1}{t_f - t_o} \int_{t_o}^{t_f} \left| \frac{E_{11}^{\text{Sph}}(t) - E_{11}^{\text{Closure}}(t)}{E_{11}^{\text{Sph}}(t)} \right| dt \times 100\% \tag{17}$$

In the present study, t_o is the initial flow time and t_f is the time when the orientation is indistinguishable from steady state. The relative error values for E_{11} presented in the first column of Table 1 quantifies the observation that the ORT, NNET, NNORT and FEC closures are more accurate in predicting the stiffness values of the processed composite, in general, than the Hybrid closure. It is clear from the results for $C_I = 10^{-2}$ that the NNORT is the best at predicting E_{11}. Similar trends exist for the time averaged relative error for each of the other stiffness components E_{22}, E_{33}, G_{23}, G_{13}, G_{12}, ν_{23}, ν_{13} and ν_{12} computed using a form similar to Equation (17), and are presented in Table 1. The closure with the greatest accuracy is bolded in Table 1 for ease of comparison. The basic trend that the NNORT is the most accurate closure holds for most of the stiffness components with the NNET, ORT and FEC having similar levels of accuracy. The exception is G_{13} where the Hybrid closure is the most accurate by a significant percentage.

Phelps and Tucker [6] presented their new ARD-RSC closure with coefficients fit based on experimental observations for a single fiber packing density and fiber aspect ratio. As observed by the numerical solution of their model in Figure 2(b) the final orientation state is not the same as was the case for the IRD model results shown in Figure 1 with $C_I = 10^{-2}$. To compare solutions between the IRD and the ARD-RSC model, we adjusted the interaction coefficient from the IRD results until the spherical harmonic solutions from both approaches yielded the same value for A_{11}. We found a value of $C_I = 3.97 \times 10^{-2}$ yielded acceptable steady state results as observed in Figure 2 for the orientation tensor. For this new interaction coefficient, the orthotropic closures and the FEC closure for the IRD again yield similar results to those of the numerically exact spherical harmonic solutions for both orientation as observed in Figure 2 and for stiffness as observed in Figure 3. Conversely, the Hybrid close tends to over predict the alignment as noted in Figure 2. As in the previous study for $C_I = 10^{-2}$, we compute the time average relative error, and as noted in Table 2 the conclusions are nearly the same as before.

3.1.1. Simple Shear Flow - Alignment Over Prediction and the Hybrid Closure

In fairness, the over prediction of alignment from the hybrid closure for the IRD flow observed in Figure 1(a) and 2(a) is not surprising. Typically in industrial processes the interaction coefficient for the hybrid closure is selected so that it retains the same steady state orientation of the principal component of the second-order orientation tensor as would be expected from the true solution. It was found that $C_I = 7.5 \times 10^{-2}$ yielded an A_{11} value nearly identical to that computed from the orthotropic closures and the spherical harmonic solution using a value of $C_I = 3.97 \times 10^{-2}$. What is interesting is how observations of the relative accuracy of exclusively the A_{11} parameter do not directly correspond with the stiffness prediction results for the hybrid closure. This is observed in Figure 3(a) for the value of E_{11} predicted from IRD flow using the various closure techniques and the spherical harmonic solution. Although the Hybrid closure results that a value of $C_I = 7.5 \times 10^{-2}$ yields a better indication of the orientation state than the value of $C_I = 3.97 \times 10^{-2}$, the reverse is true for the E_{11} stiffness component. This is counter-intuitive as it is often assumed that an accurate representation of A_{11} indicates a more accurate representation of E_{11}, which appears to not be the case in this scenario with the hybrid closure as noted in Figures 2(a) and 3(a).

To expand on this thought, we first look at the relationship for E_{11} as a function of orientation. E_{11} can be obtained from the stiffness tensor C_{ijkl}. As depicted in Equation (14), C_{ijkl} is a function of multiple components of both the second- and the fourth-order orientation tensors. Thus having only A_{ij} accurately does not insure that one will accurately represent the stiffness. In fact, accurately representing both A_{11} and A_{1111} does not necessarily indicate an accurate computation of E_{11}. E_{11} is a function of the compliance tensor S_{ijkl} through the relationship $E_{11} = 1/S_{1111}$, where the compliance tensor S_{ijkl} is the inverse of the stiffness tensor C_{ijkl}. For an orthotropic form of the stiffness tensor, the E_{11} and E_{22} components can be expressed as

$$\begin{aligned} E_{11} &= \frac{\mathrm{Det}\,(\mathbf{C})}{C_{1212}C_{1313}C_{2323}\left(C_{2222}C_{3333} - C_{2233}^2\right)} \\ E_{22} &= \frac{\mathrm{Det}\,(\mathbf{C})}{C_{1212}C_{1313}C_{2323}\left(C_{1111}C_{3333} - C_{1133}^2\right)} \end{aligned} \tag{18}$$

where $\mathrm{Det}\,(\mathbf{C})$ is the tensor determinant of the stiffness tensor C_{ijkl} and will depend on a

variety of terms from A_{ij} and A_{ijkl}. Notice that with the exception of Det $(\mathbf{C})$, E_{11} is not a function of C_{1111}, which is the only term in C_{ijkl} that contains the fourth-order orientation tensor component A_{1111}, whereas E_{22} is.

Unfortunately the form of Equation (18) with the expression Det $(\mathbf{C})$ obscures the sensitivity of the stiffness components E_{11} and E_{22} to small errors or changes in the orientation tensor. To further probe the discrepancy for the unusual behavior of the Hybrid results we take Equation (17) and look at the sensitivity of the expression to small numerical perturbations in select components of the stiffness. We do not present the sensitivity of the time averaged relative error to small changes in A_{ij} as this would explicitly impact A_{ijkl}, as A_{ijkl} is computed using a closure from A_{ij}. To compute the sensitivity, we run the complete flow history using a desired closure for $C_I = 3.97 \times 10^{-2}$ for the Spherical, Hybrid, ORT, NNORT, NNET and FEC approaches and $C_I = 7.5 \times 10^{-2}$ for the Hybrid approach. We then perturb one component of A_{iiii} (no sum on i) for the given orientation states from the simple shear flow and compute the error from Equation (17). We then use this value to define the sensitivity (derivative) of the error $\chi_{E_{11}}$ to a change in a particular fourth-order orientation tensor component as

$$\frac{d\chi_{E_{11}}}{dA_{iiii}} \simeq \frac{\chi_{E_{11}}^{\text{perturbed}} - \chi_{E_{11}}^{\text{unperturbed}}}{\Delta A_{iiii}} \tag{19}$$

where ΔA_{iiii} is a small change in a single component of A_{ijkl}. For this test, we set $\Delta A_{iiii} = 10^{-6}$ for each of the A_{1111}, A_{2222}, and A_{3333} components. In Table 3 we present the sensitivity of the error results for the material parameters E_{11}, E_{22} and E_{33} to slight variations in the fourth-order orientation tensor. Looking at the $\frac{d\chi_{E_{11}}}{dA_{iiii}}$ terms it is clear that the error for E_{11} in general is more sensitive to changes in A_{1111} relative to the E_{22} and E_{33} terms, but for the Hybrid closure with $C_I = 7.5 \times 10^{-2}$ the sensitivity of E_{11} to small changes in A_{1111} is nearly 4 times larger than that for the orthotropic closures. Small changes to the A_{2222} component effect each of the E_{11}, E_{22} and E_{33} components in similar fashions for the orthotropic closures. For the Hybrid closure a small change to A_{2222} has a significant impact on E_{22}, as well as the components E_{11} and E_{33}. It is expected that due to the preferential alignment along the x_1 axis the A_{1111} component would dominate the error for an approximated orientation state that is similar to the true orientation state, which is the case for the orthotropic closures.

But as the hybrid closure yields an orientation state that is quite dissimilar to the true orientation state, even when one orientation component is correct, the resulting confidence in the material stiffness accuracy is not easily quantified.

3.1.2. Simple Shear Flow - Differences Between IRD and ARD-RSC

As observed in Figure 2(b), for the ARD-RSC model the predicted orientation is nearly indistinguishable between the Hybrid, NNET, NNORT, ORT and FEC for the same interaction parameters $b_1 - b_5$ from Equation (6). It is worthwhile to note that for the two different fiber collision models, the IRD and the ARD-RSC, there are significant differences in the time required for the distribution to attain steady state. For the IRD model this occurs when $Gt \simeq 20 - 25$, whereas the ARD-RSC solution requires $Gt \geq 3000$. For the IRD and the ARD-RSC flows the orthotropic and the FEC closures behave in similar fashions in that they all represent, with reasonable accuracy, both the orientation state and the material stiffness parameter E_{11} as observed in Figure 3(b). The hybrid seems to reasonably represent the orientation state as shown in Figure 2(b) for the ARD-RSC flow, but the error in the E_{11} stiffness component is significant as demonstrated in Figure 3(b). The average relative error in the stiffness components is presented for the ARD-RSC results in Table 4. For most of the stiffness components the neural network closures are the most accurate for the IRD flow, whereas for the ARD-RSC flow the FEC closure is the most accurate with the ORT falling a very close second and the NNET and NNORT retaining quite reasonable accuracies. The accuracy of the Hybrid for most components is not up to the standards of the orthotropic closures.

3.2. Center-Gated Disk flow

Center-gated disk flow is indicative of the flow field near a pin gate [4, 19, 25], and regularly occurs in industrial processes. In this type of flow, the fiber suspension enters the mold through a pin gate and flows radially outward where the velocity vector $\mathbf{v} = (v_r, v_\theta, v_z)$ is a function of both the gap height 2b between the wall of the mold and the radial distance r from the gate. The velocity field and the velocity gradient of a center gated disk for a

Newtonian solvent may be represented as

$$
\begin{aligned}
v_r &= \frac{3Q}{8\pi rb}\left(1-\left(\frac{z}{b}\right)^2\right), \qquad v_\theta = v_z = 0 \\
\frac{\partial v_i}{\partial x_j} &= \frac{3Q}{8\pi rb}\begin{bmatrix} -\frac{1}{r}\left(1-\frac{z^2}{b^2}\right) & 0 & -\frac{2}{b}\frac{z}{b} \\ 0 & \frac{1}{r}\left(1-\frac{z^2}{b^2}\right) & 0 \\ 0 & 0 & 0 \end{bmatrix}
\end{aligned} \tag{20}
$$

where z is the gap height location between the mold walls with $z = 0$ taken to be the mid-plane between the mold walls and Q is the volumetric flow rate. In practice, one would couple the flow kinetics with the fiber orientation kinematics (see e.g., [21, 22, 19] for how this might be done), but in the present context, to retain the focus on purely orientational effects, we leave the coupled problem for various diffusion models to a future study. We made predictions for the streamline along $z/b = 5/10$ with an initial isotropic fiber orientation at $r/b = 1$. The result for $\mathbf{A}$ from both the IRD and the ARD-RSC fiber interaction models is shown in Figure 4, and as in the previous example $C_I = 3.97 \times 10^{-2}$ (except for the Hybrid, where we used $C_I = 7.5 \times 10^{-2}$) to insure the same steady state orientation between the two fiber interaction models. The observations are quite similar to those from the simple shear flow where all of the closures reasonably predict the alignment state for both the IRD and the ARD-RSC results. For both the IRD and ARD-RSC flow, the Hybrid, NNET, NNORT, ORT and FEC appear to give quite similar results with the NNORT appearing to yield a slightly better prediction of $\mathbf{A}$. It is interesting to note the predicted material stiffness from each of the closures over the two different diffusion model flows, as indicated in Figure 5 for E_{11}, as a function of radial distance in the mold. Notice the large initial dip in the E_{11} component from the IRD model, which is due to the large out-of-plane shear.Conversely, for the ARD-RSC model, this same large dip does not occur. This is not surprising as the ARD-RSC model slows the rate of change in the orientation whereby the out-of-plane shearing only occurs during a small portion of the mold filling, and for increasing values of r/b the flow is dominated by the radial shearing. Therefore this dip would not be expected to occur in the ARD-RSC flow model. As in the simple shear flow, the Hybrid predicts the A_{11} component for both the IRD and the ARD-RSC flow reasonably well, but significantly under predicts E_{11}. The stiffness prediction of E_{11} from the ARD-RSC flow is noted in

Figure 5(b) where the orientation results from each of the orthotropic and FEC closures mapped over reasonably well to the stiffness predictions with similar trends. The error for each of the stiffness components are presented in Table 5 for the IRD model, and unlike the shear results no closure is clearly the best between the NNET, NNORT, ORT and FEC as each produce similar error results for each of the investigated stiffness components with one or the other performing better for various components. It is striking to note that with the exception of G_{23} and ν_{13} the hybrid closure has difficulty in representing the stiffness.

3.3. Thin Geometry Prediction

For the present study we will focus on the lubrication region of a thin plaque and far from the mold edges. This flow is not a true filling calculation as both the fountain effect and thermal gradients are neglected. For industrial simulations, the interested reader should investigate Bay and Tucker [44]. The following example is intended to highlight the differences between the diffusion models while retaining orientational similarities with a plaque molded part, i.e., a less oriented core and a slightly oriented shell layer. The thin cavity is defined as having length $l = 10cm$ and thickness of $h = 3.2mm$. The flow is fully developed and pressure driven, with the viscous properties of HDPE polymer (a pseudo plastic). The shear stress tensor of a pseudo plastic is defined, (see e.g., [45]), by

$$\tau_{ij} = 2K|2\Gamma_{kl}\Gamma_{kl}|^{(\frac{n-1}{2})}\Gamma_{ij} \quad \text{sum on } k \text{ and } l \tag{21}$$

$$\Gamma_{ij} = \frac{1}{2}(\frac{\partial v_i}{\partial x_j} + \frac{\partial v_j}{\partial x_i}) \tag{22}$$

and using Equation (21) and (22), the shear stress τ_{13} in the thin cavity, with x_1 being the flow direction and x_3 the direction of shear, is

$$\tau_{13} = 2K|\frac{\partial v_1}{\partial x_3}|^{n-1}\frac{\partial v_1}{\partial x_3} \tag{23}$$

where K is the flow consistency index in units of $Pa.s^n$ and n is the flow behavior index (dimensionless). Using the differential equation for the momentum flux, the second order partial differential equation of a fully developed simple shear flow in a thin cavity can be solved to yield the average velocity profile of (see e.g., [11] for the full derivation)

$$v_1 = \frac{n}{n+1}\left(\frac{(p_1 - p_2)}{KL}\right)^{1/n}\left[\left(\frac{h}{2}\right)^{1+\frac{1}{n}} - |x_3|^{1+\frac{1}{n}}\right] \tag{24}$$

Note, the velocity does not change along the flow direction x_1, but varies in the x_3 direction. In Equation (24), h is the the thickness of the mold cavity and p_1 and p_2 are the inlet and outlet pressures respectively. For our prediction we selected a pressure differential of 100 psi (69MPa) , $K = 2 \times 10^{-4}$ and $n = 0.41$.

Observing the significant difference in the elastic properties predicted, using both of the two fiber interaction models, will lend insight to experimentalists for choosing which diffusion model is more applicable for their system, and should be the scope of a future study. The longitudinal Young's moduli E_{11} are presented in Figure 6 in the left and right column for, respectively, the IRD and the ARD-RSC model results. In each cavity, the flow enters from the left side with an initial isotropic orientation state. Along the walls the fibers quickly align but within the core region the fibers take a significantly longer period to reach any noticeable change in the alignment as observed by the low E_{11} values. Notice for the same geometry and fluid flow profile the two diffusion models demonstrate a remarkable difference in the spatially varying E_{11} values. The IRD model predicts somewhat uniform longitudinal elastic young modulus just a few millimeters from the inlet, whereas the ARD-RSC has considerable spatial inhomogeneity.

The closure effects for each of the fiber interaction models is also very interesting. For example there is some difference in E_{11} values from the closure results as compared to the spherical solution for the IRD interaction model, as observed by viewing the colors in Figure 6. For the ARD-RSC flow the Hybrid result difference is quite drastic, therefore, having the orientation correctly (as defined by $\mathbf{A}$ alone) is not sufficient for capturing the stiffness. The FEC results on the other-hand (where the FEC and ORT yield visually identical results in this example) are quite stable for both fiber interaction models, lending further motivation to accepting the newer closure.

3.4. Eigenfrequency Analysis

We decided to carry out investigation on the natural frequencies of the simulated thin plaque in the hopes of observing differences between diffusion models. This was originally done in the hope that macroscopic experimental analysis techniques might be developed to quantify the choice of diffusion model, and in particular the rate of alignment within a part.

To carry out this eigenfrequency analysis, COMSOL Multiphysics was used to call MATLAB scripts containing the spatially varying stiffness properties based on the orientation results from solving Equation (4) and (5) for the IRD and the ARD-RSC models respectively. A density of 1000 kg/m^3 with a part depth of 1.27mm, height of 3.2mm and length of 10cm was used for predicting the eigenfrequency of a thin plaque where the inlet side of the plaque is clamped. The results for the first five natural frequencies using the Hybrid and the FEC closures (where NNET, NNORT, and ORT results were nearly indistinguishable with that of the FEC) as well as the spherical harmonics solution are shown in Figure 7(a) for the IRD model and in Figure 7(b) for the ARD-RSC model result. The FEC and Hybrid closures yield very similar frequency predictions as that of the spherical harmonics solution for both models. Clearly from Figure 7 there is very little difference in the natural frequencies for the two fiber interaction models, even though there is a significant difference in the stiffness predictions as noted in Figure 6. This seemingly counterintuitive observation warrants further discussion. The finite element model for the natural frequency prediction can be expressed as (see e.g., [11])

$$(\mathbf{K}\mathbf{M}^{-1} - \omega^2\mathbf{I})\ \mathbf{\Delta} = 0 \tag{25}$$

where ω is the natural frequency, $\mathbf{K}$ is the stiffness tensor and $\mathbf{M}$ is the mass matrix. From Equation (25) it can be shown that if the value of stiffness is doubled the eigenfrequency will only increase by $\sqrt{2}$ (see e.g., [46, 11]). Consequently, based on the observations of the moduli in Figure 6 the differences in the stiffness is well below even a factor of two, and it is not significant enough to warrant the use of natural frequencies to determine the fiber interaction model for a given fiber suspension.

3.5. Flexural Modulus Analysis

The eigenfrequency is obviously insensitive to the fiber orientation change predicted by the two models. An alternative is the flexural modulus test for the thin plaque. The flexural modulus is a measure of stiffness of a part and is often used to characterize reinforced plastics. The flexural modulus (E_b) is typically referred to as the slope of the flexural stress against the flexural strain in a three-point bending test [47], and is often defined as $E_b = FL^3/4bh^3$, where F is the applied load, L is the length or span of support, b is the depth of the plaque,

h is the thickness of the plaque. The dimension of the part used for our simulated flexural test was length×depth×thickness of 10cm×1.27mm×3.2mm chosen in accordance with the ASTM D790 test fixture [47]. The simulated test was carried out for the IRD and the ARD-RSC models using the FEC and Hybrid closures along with the spherical harmonic results. The results for ORT, NNET and NNORT, are not presented because their results and that of the FEC closure are similar. The finite element analysis was performed using COMSOL for the three point bend tests. The properties of the part vary spatially, and a single test cannot be used to capture the changes in the stiffness. A study is performed at regular intervals in the part to mimic the 3 point bend test fixture, and are presented in Figure 8. To capture the spatial variation in the stiffness, the three point bend test was performed at various positions along the plaque, but each test was for the same fixed interval of 1 cm. This interval was chosen as it was nearly a factor of 10 greater than the part thickness. If the interval is increased too much, it will be harder to capture local effects, whereas if the interval is decreased significantly the concept of flexural modulus becomes ambiguous. From the figure, it can be observed that the flexural moduli values predicted form the ARD-RSC are significantly different from those predicted by the IRD model. The ARD-RSC result shows significant changes in the flexural modulus along the length of the beam whereas for the IRD model, there was no significant change.

We hypothesize that testing the flexural modulus for each section of a molded composite may be a way to determine which of the two rotary diffusion models is appropriate. For example, if the percent change in flexural modulus along the global length of the thin plaque is very low (i.e no significant change), the IRD model may be the appropriate model. On the other hand, if there is considerable change in the flexural modulus along the length the ARD-RSC model would be appropriate, and possibly this approach could be used to quantify the parameter κ used in the ARD-RSC equation of motion. A tangential observation is that of the Hybrid closure flexural modulus, which increases and then decreases as we move along the length of the thin plaque, contrary to the predictions for the FEC and the spherical results. The explanation we found for this difference is that the shear modulus G_{13} plays a large role in the value of the flexural modulus. For the Hybrid closure G_{13} behaved in a different manner relative to the FEC and the spherical results. For the Hybrid results,

G_{13} showed an initial increase and then a continuous and significant decrease, unlike the continuous and gradual decrease observed for the FEC and the spherical results.

4. Conclusions

This paper presents two different rotary diffusion mathematical models used for predicting flow induced orientation of an injection molded short fiber reinforced thermoplastic. Several closure approximation methods were used to solve the second-order orientation tensor equation of motion. In general it was observed that the FEC and the orthotropic closures performed quite well for each of the flows investigated, with the FEC generally providing a small improvement in accuracy relative to the orthotropic closures. In this paper, we demonstrated that using the second-order orientation tensor to infer the accuracy in obtaining a particular stiffness component may be insufficient. In particular, observe the solution from the ARD-RSC model where the **A** components from each of the closures are quite similar, but the resulting fourth-order stiffness tensor has a considerable difference between the closure predictions with the orthotropic and FEC closures performing with the greatest accuracy. This paper presented the eigenfrequency approach for possible use in determining which diffusion model for fiber interactions is more appropriate for a given fiber suspension, but based on the results presented it appears this is not a viable approach for industrial use in selecting a diffusion model. Conversely, the flexural modulus results are quite promising, and our results indicate that this may be a viable experimental approach to confirm or refute a particular diffusion model and may even aid in the selection of the empirical parameters for the diffusion model. Our study revealed that there is significant difference between the ARD-RSC and the IRD models, which provide motivation for further studies to validate which fiber interaction model is appropriate for commercial predictions of the resulting stiffness of injection molded short-fiber reinforced composites.

5. Acknowledgements

The authors gratefully acknowledge support from N.S.F. via grant C.M.M.I. 0727399 as well as Baylor University through their new faculty start-up assistance. The authors are

also exceedingly grateful to the reviewers and their suggestion to investigate the flexural modulus.

[1] F. Folgar, C. Tucker, Orientation Behavior of Fibers in Concentrated Suspensions, Journal of Reinforced Plastics and Composites 3 (1984) 98–119.

[2] S. Advani, C. Tucker, The Use of Tensors to Describe and Predict Fiber Orientation in Short Fiber Composites, Journal of Rheology 31 (8) (1987) 751–784.

[3] R. Bay, Fiber Orientation in Injection Molded Composites: A Comparison of Theory and Experiment, Ph.D. thesis, University of Illinois at Urbana-Champaign (August 1991).

[4] J. S. Cintra, C. Tucker, Orthotropic Closure Approximations for Flow-Induced Fiber Orientation, Journal of Rheology 39 (6) (1995) 1095–1122.

[5] D. Koch, A Model for Orientational Diffusion in Fiber Suspensions, Physics of Fluids 7 (8) (1995) 2086–2088.

[6] J. Phelps, C. Tucker, An Anisotropic Rotary Diffusion Model for Fiber Orienation in Short- and Long Fiber Thermoplastics, Journal of Non-Newtonian Fluid Mechanics 156 (2009) 165–176.

[7] G. Jeffery, The Motion of Ellipsoidal Particles Immersed in a Viscous Fluid, Proceedings of the Royal Society of London A 102 (1923) 161–179.

[8] S. Advani, Prediction of Fiber Orientation During Processing of Short Fiber Composites, Ph.D. thesis, University of Illinois at Urbana-Champaign (August 1987).

[9] D. Jack, D. Smith, An Invariant Based Fitted Closure of the Sixth-order Orientation Tensor for Modeling Short-Fiber Suspensions, Journal of Rheology 49 (5) (2005) 1091–1116.

[10] N. Qadir, D. Jack, Modeling Fibre Orientation in Short Fibre Suspensions Using the Neural Network-Based Orthotropic Closure, Composites, Part A 40 (2009) 1524–1533.

[11] B. Agboola, Investigation of Dense Suspension Rotary Diffusion Models for Fiber Orientation Predictions during Injection Molding of Short-Fiber Reinforced Polymeric Composites, Master's thesis, Baylor University (August 2011).

[12] Montgomery-Smith, S.J., D. Jack, D. Smith, A Systematic Approach to Obtaining Numerical Solutions of Jefferys Type Equations using Spherical Harmonics, Composites, Part A 41 (2010) 827–835.

[13] M. Doi, Molecular dynamics and rheological properties of concentrated solutions of rodlike polymers in isotropic and liquid crystalline phases, Journal of Polymer Science Part B Polymer Physics 19 (1981) 229–243.

[14] G. Hand, A Theory of Anisotropic Fluids, Journal of Fluid Mechanics 13 (1) (1962) 33–46.

[15] V. Verleye, F. Dupret, Prediction of Fiber Orientation in Complex Injection Molded Parts, in: Developments in Non-Newtonian Flows, 1993, pp. 139–163.

[16] D. Jack, B. Schache, D. Smith, Neural Network Based Closure for Modeling Short-Fiber Suspensions, Polymer Composites 31 (7) (2010) 1125–1141.

[17] Montgomery-Smith, S.J., W. He, D. Jack, D. Smith, Exact Tensor Closures for the Three Dimensional Jeffery's Equation, Journal of Fluid Mechanics 680 (2011) 321–335.

[18] Montgomery-Smith, S.J., D. Jack, D. Smith, The Fast Exact Closure for Jeffery's Equation with Diffusion, Journal of Non-Newtonian Fluid Mechanics 166 (2011) 343–353.

[19] B. VerWeyst, T. C. III, Fiber Suspensions in Complex Geometries: Flow-Orientation Coupling, The Canadian Journal of Chemical Engineering 80 (2002) 1093–1106.

[20] J. Wang, J. O'Gara, C. Tucker, An Objective Model for Slow Orientation Kinetics in Concentrated Fiber Suspensions: Theory and Rheological Evidence, Journal of Rheology 52 (5) (2008) 1179–1200.

[21] S. Dinh, R. Armstrong, A Rheological Equation of State for Semiconcentrated Fiber Suspensions, Journal of Rheology 28 (3) (1984) 207–227.

[22] G. I. Lipscomb, M. Denn, D. Hur, D. Boger, Flow of Fiber Suspensions in Complex Geometries, Journal of Non-Newtonian Fluid Mechanics 26 (1988) 297–325.

[23] D. Chung, T. Kwon, Numerical Studies of Fiber Suspensions in an Axisymmetric Radial Diverging Flow: The Effects of Modeling and Numerical Assumptions, Journal of Non-Newtonian Fluid Mechanics 107 (2002) 67–96.

[24] A. Eberle, G. Velez-Garcia, D. Baird, P. Wapperom, Fiber orientation kinetics of a concentrated short glass fiber suspension in startup of simple shear flow, Journal of Non-Newtonian Fluid Mechanics 165 (2010) 110–119.

[25] D. Jack, D. Smith, Elastic Properties of Short-Fiber Polymer Composites, Derivation and Demonstration of Analytical Forms for Expectation and Variance from Orientation Tensors, Journal of Composite Materials 42 (3) (2008) 277–308.

[26] E. Caselman, Elastic Property Prediction of Short Fiber Composites Using a Uniform Mesh Finite Element Method, Master's thesis, University of Missouri - Columbia (December 2007).

[27] A. Gusev, M. Heggli, H. Lusti, P. Hine, Orientation Averaging for Stiffness and Thermal Expansion of Short Fiber Composites, Advanced Engineering Materials 4 (12) (2002) 931–933.

[28] A. Gusev, H. Lusti, P. Hine, Stiffness and Thermal Expansion of Short Fiber Composites with Fully Aligned Fibers, Advanced Engineering Materials 4 (12) (2002) 927–930.

[29] N. Nguyen, S. Bapanapalli, V. Kunc, J. Phelps, C. Tucker, Prediction of the Elastic-Plastic Stress/Strain Response for Injection-Molded Long-Fiber Thermoplastics, Journal of Composite Materials 43 (3) (2009) 217–246.

[30] R. B. Bird, C. Curtiss, R. C. Armstrong, O. Hassager, Dynamics of Polymeric Liquids, 2nd Edition, Vol. 2: Kinetic Theory, John Wiley & Sons, Inc., New York, NY, 1987.

[31] D. Zhang, D. Smith, D. Jack, S. Montgomery-Smith, Numerical Evaluation of Single Fiber Motion for Short-Fiber-Reinforced Composite Materials Processing, Journal of Manufacturing Science and Engineering 133 (5) (2011) 051002–9.

[32] D. Jack, Advanced Analysis of Short-fiber Polymer Composite Material Behavior, Ph.D. thesis, University of Missouri - Columbia (December 2006).

[33] X. Fan, N. Phan-Thien, R. Zheng, A Direct Simulation of Fibre Suspensions, Journal of Non-Newtonian Fluid Mechanics 74 (1998) 113–135.

[34] N. Phan-Thien, X.-J. Fan, R. Tanner, R. Zheng, Folgar-Tucker Constant for a Fibre Suspension in a Newtonian Fluid, Journal of Non-Newtonian Fluid Mechanics 103 (2002) 251–260.

[35] S. Advani, C. Tucker, Closure Approximations for Three-Dimensional Structure Tensors, Journal of Rheology 34 (3) (1990) 367–386.

[36] K.-H. Han, Y.-T. Im, Numerical Simulation of Three-Dimensional Fiber Orientation in Short-Fiber-Reinforced Injection-Molded Parts, Journal of Materials Processing Technology 124 (2002) 366–371.

[37] D. Chung, T. Kwon, Improved Model of Orthotropic Closure Approximation for Flow Induced Fiber Orientation, Polymer Composites 22 (5) (2001) 636–649.

[38] D. Chung, T. Kwon, Invariant-Based Optimal Fitting Closure Approximation for the Numerical Prediction of Flow-Induced Fiber Orientation, Journal of Rheology 46 (1) (2002) 169–194.

[39] D. Dray, P. Gilormini, G. Regnier, Comparison of Several Closure Approximations for Evaluating the Thermoelastic Properties of an Injection Molded Short-Fiber Composite, Composites Science and Technology 67 (7-8) (2007) 1601–1610.

[40] A. Gusev, P. Hine, W. I.M., Fiber Packing and Elastic Properties of a Transversely Random Unidirectional Glass/Epoxy Composite, Composites Science and Technology 60 (2000) 535–541.

[41] C. Tucker, E. Liang, Stiffness Predictions for Unidirectional Short-Fiber Composites: Review and Evaluation, Composites Science and Technology 59 (1999) 655–671.

[42] G. Tandon, G. Weng, The Effect of Aspect Ratio of Inclusions on the Elastic Properties of Unidirectionally Aligned Composites, Polymer Composites 5 (4) (1984) 327–333.

[43] R. Jones, Mechanics of Composite Materials: Second Edition, Taylor and Francis, Inc., Philadelphia, PA, 1999.

[44] R. Bay, C. Tucker, Fiber Orientation in Simple Injection Moldings: Part 1 - Theory and Numerical Methods, in: V. Stokes (Ed.), Plastics and Plastic Composites: Material Properties, Part Performance, and Process Simulation, ASME 1991, Vol. **29**, American Society of Mechanical Engineers, 1991, pp. 445–471.

[45] A. Ishak, N. Bachok, Power-Law Fluid Flow On a Moving Wall, European Journal of Scientific Research 34 (1) (2009) 55–60.

[46] J. Reddy, An Introduction to the Finite Element Method, Third Edition, McGraw-Hill, New York, NY, 2006.

[47] ASM Handbook: Mechanical Testing and Evaluation , Vol. **8**, ASM International, West Sussex, England, 2000.

Table 1: Percent relative error for the material stiffness results from a simple shear flow for the IRD results with $C_I = 0.01$ and $a_e = 10$ (bold font indicates the result with the greatest accuracy).

	$\chi_{E_{11}}$	$\chi_{E_{22}}$	$\chi_{E_{33}}$	$\chi_{G_{23}}$	$\chi_{G_{13}}$	$\chi_{G_{12}}$	$\chi_{\nu_{12}}$	$\chi_{\nu_{13}}$	$\chi_{\nu_{23}}$
Hybrid	10.7	11.7	5.1	6.8	**0.3**	3.7	11.0	2.2	4.3
ORT	4.8	0.6	**0.2**	1.3	2.7	2.6	0.5	1.1	2.1
NNET	4.3	1.7	0.5	1.2	1.5	**1.6**	1.1	1.4	2.0
NNORT	**3.7**	**0.4**	**0.2**	**1.0**	1.8	**1.6**	**0.2**	**0.9**	**1.5**
FEC	4.8	0.6	**0.2**	1.3	2.7	2.6	0.5	1.1	2.1

Table 2: Percent average relative error for the material stiffness results from a simple shear flow for the IRD results with $C_I = 0.0397$ and $a_e = 10$ (bold font indicates the result with the greatest accuracy).

	$\chi_{E_{11}}$	$\chi_{E_{22}}$	$\chi_{E_{33}}$	$\chi_{G_{23}}$	$\chi_{G_{13}}$	$\chi_{G_{12}}$	$\chi_{\nu_{12}}$	$\chi_{\nu_{13}}$	$\chi_{\nu_{23}}$
Hybrid ($C_I = 3.97 \times 10^{-2}$)	**1.4**	14.1	7.5	5.5	5.7	10.4	18.7	1.5	**0.9**
Hybrid ($C_I = 7.5 \times 10^{-2}$)	9.3	10.1	5.7	0.8	8.2	10.2	12.1	1.1	3.4
ORT	2.6	**0.1**	0.4	**0.5**	2.0	1.6	0.5	**1.0**	1.4
NNET	2.5	0.3	**0.2**	**0.5**	**1.8**	**1.0**	0.4	1.3	1.4
NNORT	2.6	0.1	0.4	**0.5**	2.0	1.5	**0.3**	1.1	1.4
FEC	2.6	**0.2**	0.5	0.6	2.0	1.7	0.5	**1.0**	1.3

Table 3: Sensitivity of the average relative error to select fourth-order orientation tensor components for the material stiffness results from a simple shear flow for the IRD results with $C_I = 0.0397$ and $a_e = 10$.

	$\frac{d\chi_{E_{11}}}{A_{1111}}$	$\frac{d\chi_{E_{22}}}{A_{1111}}$	$\frac{d\chi_{E_{33}}}{A_{1111}}$	$\frac{d\chi_{E_{11}}}{A_{2222}}$	$\frac{d\chi_{E_{22}}}{A_{2222}}$	$\frac{d\chi_{E_{33}}}{A_{2222}}$	$\frac{d\chi_{E_{11}}}{A_{3333}}$	$\frac{d\chi_{E_{22}}}{A_{3333}}$	$\frac{d\chi_{E_{33}}}{A_{3333}}$
Hybrid ($C_I = 3.97 \times 10^{-2}$)	-1.5	-1.9	1	3.3	-19.1	-5.2	-0.1	-3.4	-10.9
Hybrid ($C_I = 7.5 \times 10^{-2}$)	-9.5	-3.5	-1.5	-4.8	-13.6	-1.7	-1.4	-0.8	-8.4
ORT	-2.6	-0.4	-0.7	-0.5	-0.2	0.6	-0.7	0.4	-0.5
NNET	-2.6	0.4	-0.6	-0.3	-0.4	0.6	-0.7	-0.6	-0.3
NNORT	-2.6	0.4	-0.7	-0.4	-0.2	0.7	-0.7	-0.5	-0.5
FEC	-2.6	-0.5	-0.7	-0.5	-0.2	0.6	-0.7	0.5	-0.7

Table 4: Percent average relative error for the material stiffness results from a simple shear flow for the ARD-RSC results with $a_e = 10$ (bold font indicates the result with the greatest accuracy).

	$\chi_{E_{11}}$	$\chi_{E_{22}}$	$\chi_{E_{33}}$	$\chi_{G_{23}}$	$\chi_{G_{13}}$	$\chi_{G_{12}}$	$\chi_{\nu_{12}}$	$\chi_{\nu_{13}}$	$\chi_{\nu_{23}}$
Hybrid	20.9	19.8	3.6	0.9	4.0	28.1	37.0	18.3	15.2
ORT	**1.6**	1.6	**0.3**	0.4	**0.6**	0.8	**0.9**	**0.6**	1.0
NNET	2.2	1.4	0.6	1.2	1.7	**0.7**	1.1	0.9	1.0
NNORT	2.2	**1.2**	0.7	1.7	2.7	0.8	1.6	1.9	**0.6**
FEC	**1.6**	1.6	**0.3**	**0.3**	**0.6**	0.8	**0.9**	**0.6**	0.9

Table 5: Percent average relative error for the material stiffness results for the center-gated disc, $z/b = 5/10$ for the IRD results with $C_I = 0.0397$ and $a_e = 10$ (bold font indicates the result with the greatest accuracy).

	$\chi_{E_{11}}$	$\chi_{E_{22}}$	$\chi_{E_{33}}$	$\chi_{G_{23}}$	$\chi_{G_{13}}$	$\chi_{G_{12}}$	$\chi_{\nu_{12}}$	$\chi_{\nu_{13}}$	$\chi_{\nu_{23}}$
Hybrid ($C_I = 7.5 \times 10^{-2}$)	9.4	10.7	5.7	1.4	8.3	10.2	12.9	**1.0**	3.4
ORT	2.8	0.2	0.5	**0.6**	2.0	1.4	0.3	1.2	1.4
NNET	**2.7**	0.4	**0.4**	0.7	**1.9**	**0.8**	0.7	1.5	**1.3**
NNORT	2.8	0.2	0.5	0.7	**1.9**	1.3	**0.2**	1.3	1.4
FEC	2.8	**0.1**	0.6	0.8	**1.9**	1.5	0.3	1.2	**1.3**

Table 6: Percent average relative error for the material stiffness results for the center-gated disc, $z/b = 5/10$ for the ARD-RSC results with $a_e = 10$ (bold font indicates the result with the greatest accuracy).

	$\chi_{E_{11}}$	$\chi_{E_{22}}$	$\chi_{E_{33}}$	$\chi_{G_{23}}$	$\chi_{G_{13}}$	$\chi_{G_{12}}$	$\chi_{\nu_{12}}$	$\chi_{\nu_{13}}$	$\chi_{\nu_{23}}$
Hybrid	21.1	20.2	3.6	1.0	3.8	28.3	37.6	18.7	15.5
ORT	**1.5**	1.6	**0.3**	0.5	**0.6**	0.7	**0.9**	**0.6**	1.0
NNET	2.3	**1.1**	0.6	1.2	1.5	**0.5**	1.1	1.1	0.8
NNORT	2.1	**1.1**	0.7	1.8	2.6	0.7	1.7	2.0	**0.6**
FEC	**1.5**	1.6	**0.3**	**0.3**	**0.6**	0.7	**0.9**	**0.6**	0.9

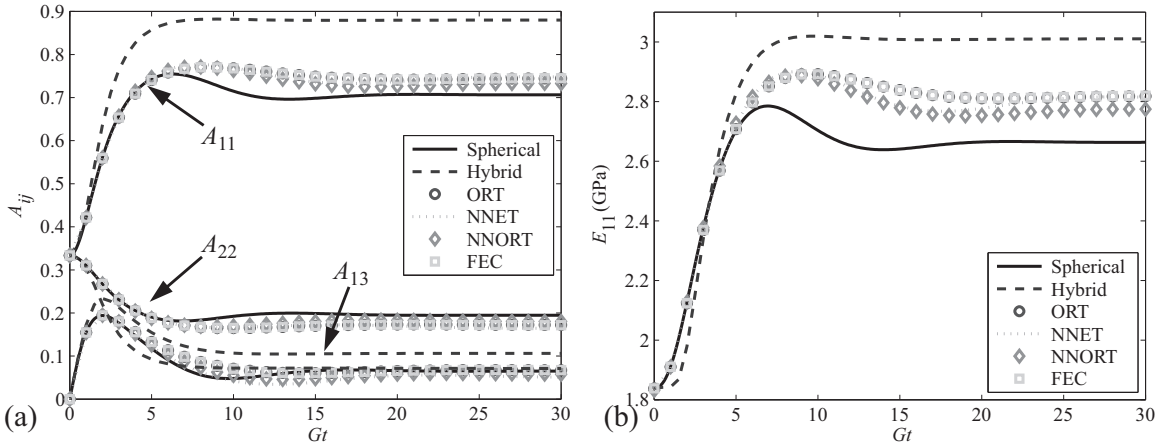

Figure 1: Simple shear flow with $C_I = 0.01$ and $a_e = 10$ for the IRD model, (a) fiber orientation and (b) the resulting longitudinal modules E_{11}.

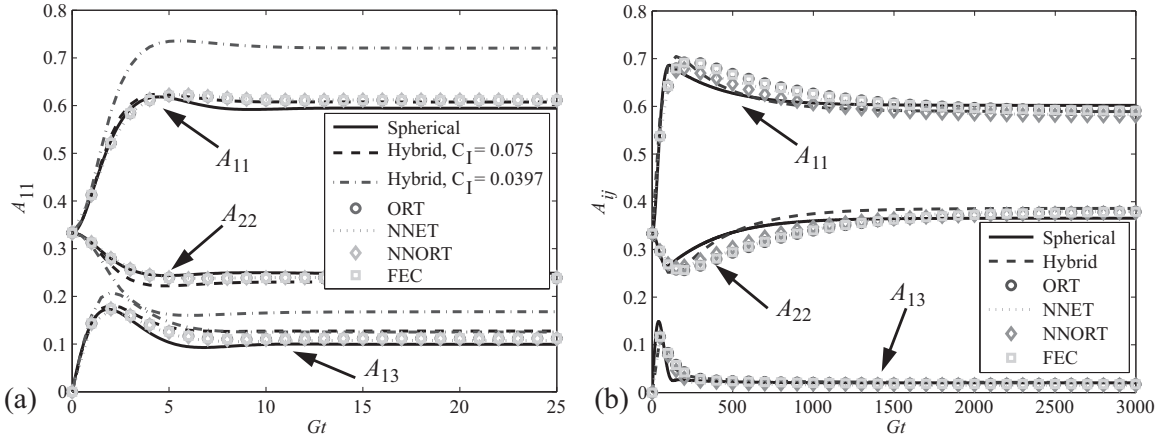

Figure 2: Comparison of change in fiber orientation in simple-shear flow for (a) the IRD model with $C_I = 0.0397$ and $a_e = 10$ and (b) the ARD-RSC model with $a_e = 10$.

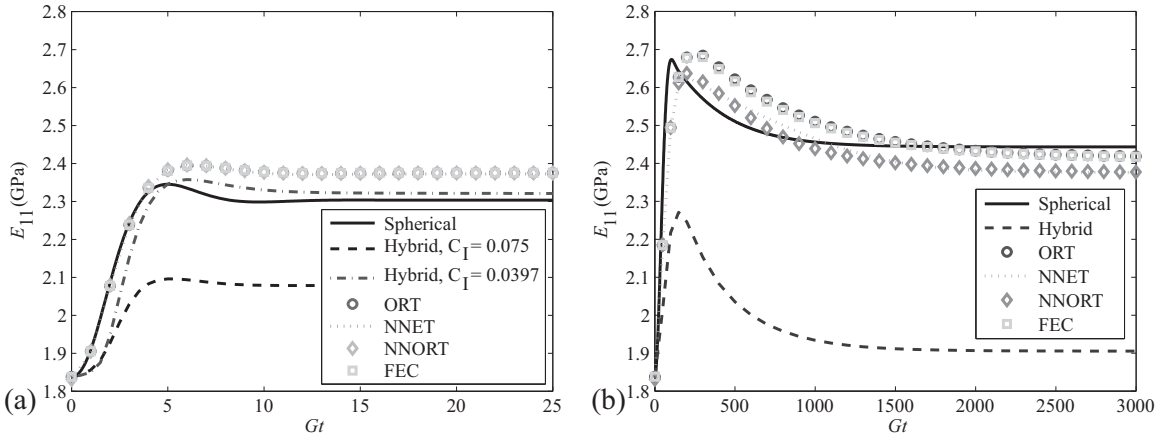

Figure 3: Comparison of longitudinal modulus E_{11} along a streamline for a solidified part fabricated under simple shear flow at select processing times for (a) the IRD model with $C_I = 0.0397$ and $a_e = 10$ and (b) the ARD-RSC model with $a_e = 10$.

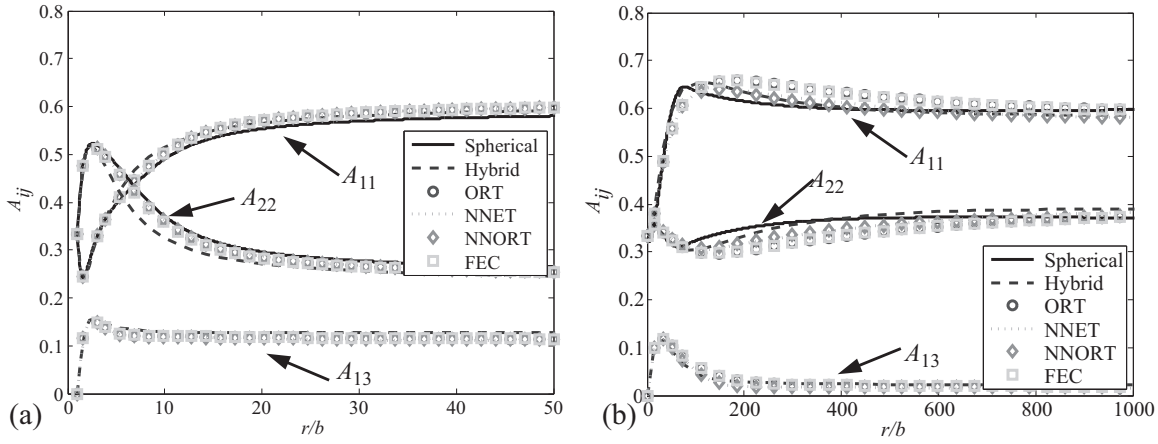

Figure 4: Comparison of change in fiber orientation in center gated disk flow for $z/b = 5/10$ (a) the IRD model with $C_I = 0.0397$ (Hybrid, $C_I = 7.5 \times 10^{-2}$) and $a_e = 10$ and (b) the ARD-RSC model with $a_e = 10$

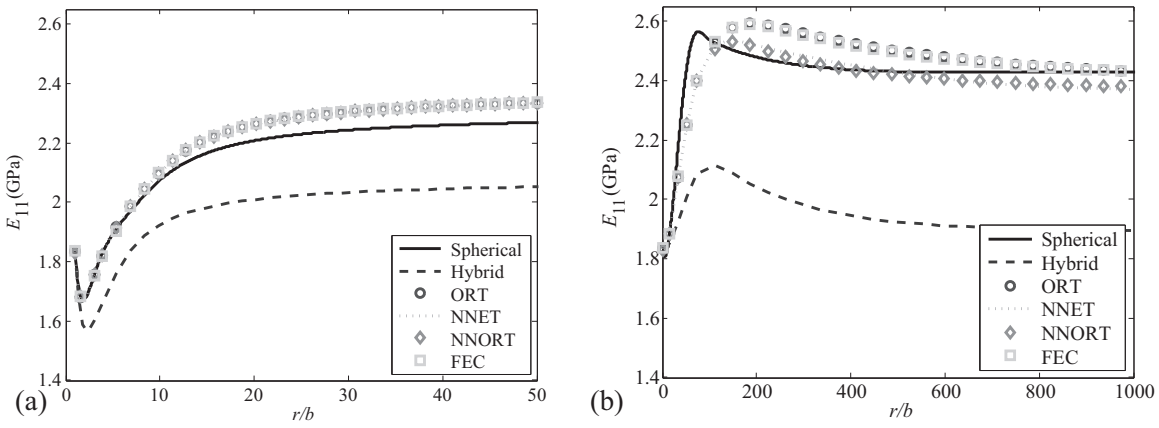

Figure 5: Comparison of the longitudinal modulus E_{11} along a streamline for a solidified part fabricated under center gated disk $z/b = 5/10$ flow at select processing times for (a) the IRD model with $C_I = 0.0397$ (Hybrid, $C_I = 7.5 \times 10^{-2}$) and $a_e = 10$ and (b) the ARD-RSC model with $a_e = 10$.

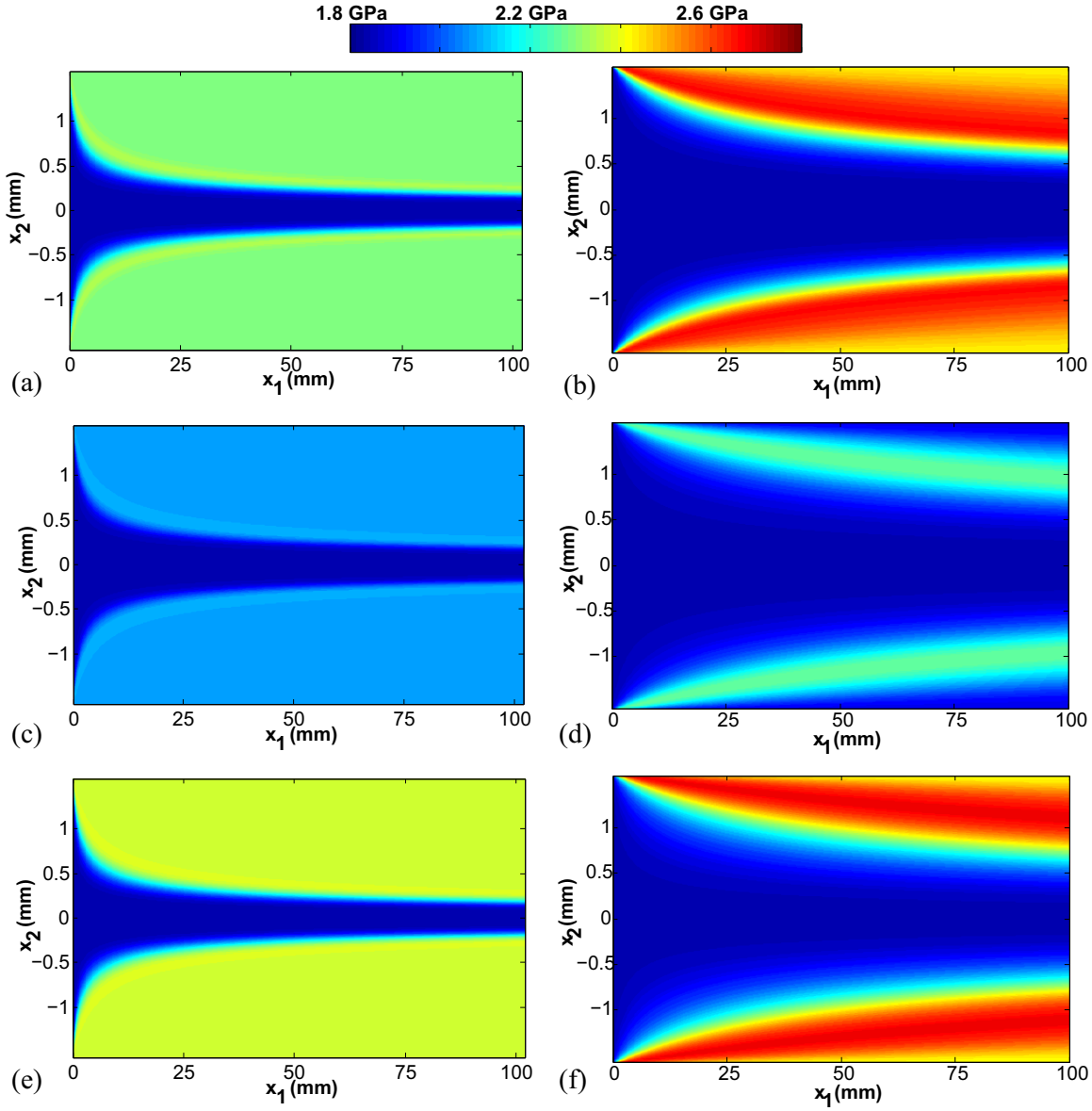

Figure 6: Comparison of the longitudinal modulus E_{11} for a processed thin plaque for the IRD ($C_I = 3.97 \times 10^{-2}$ and $a_e = 10$) and the ARD-RSC ($a_e = 10$) models. (a) IRD - Spherical Harmonic Solution, (b) ARD-RSC - Spherical Harmonic Solution, (c) IRD - Hybrid Closure with $C_I = 7.5 \times 10^{-2}$, (d) ARD-RSC - Hybrid Closure, (e) IRD - FEC Closure, and (f) ARD-RSC - FEC Closure.

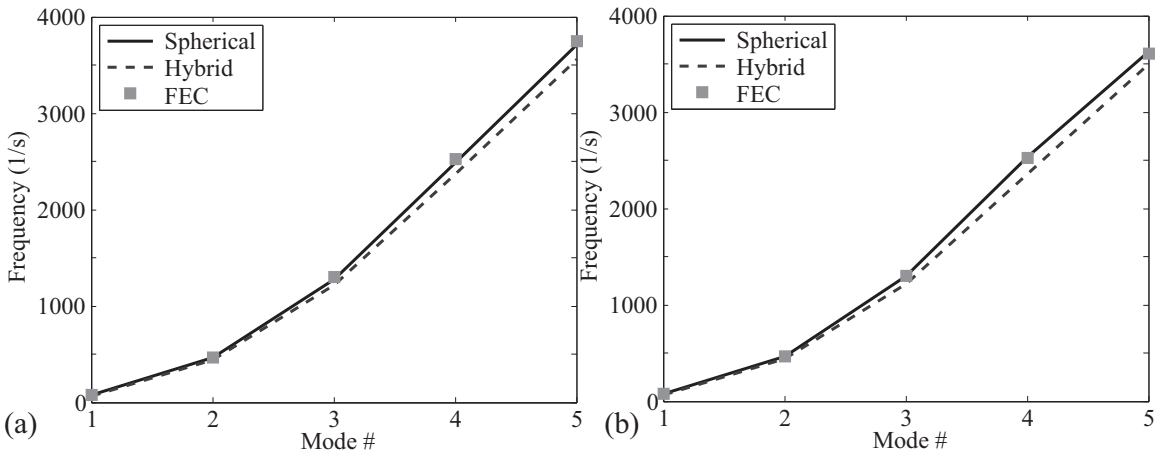

Figure 7: Comparison of the first five natural frequencies for a processed thin plaque for (a) the IRD model with $C_I = 3.97 \times 10^{-2}$ (Hybrid, $C_I = 7.5 \times 10^{-2}$) and $a_e = 10$ and (b) the ARD-RSC model with $a_e = 10$.

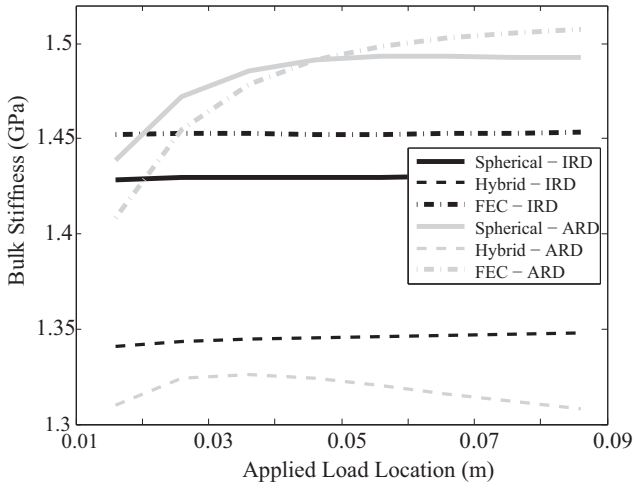

Figure 8: Flexural modulus as a function of distance from the plaque inlet as predicted from the spherical harmonic, Hybrid and FEC results for both diffusion models.